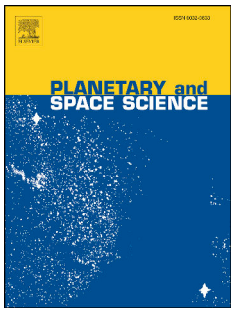

Granular sample collection simulation via counter rotating wheels sampler for small-sized system at reduced gravity environment

E. Sitepu, D. Cullen

PII: S0032-0633(23)00147-2

DOI: https://doi.org/10.1016/j.pss.2023.105778

Reference: PSS 105778

To appear in: *Planetary and Space Science*

Received Date: 3 April 2023

Revised Date: 19 June 2023

Accepted Date: 7 September 2023

Please cite this article as: Sitepu, E., Cullen, D., Granular sample collection simulation via counter rotating wheels sampler for small-sized system at reduced gravity environment, *Planetary and Space Science* (2023), doi: https://doi.org/10.1016/j.pss.2023.105778.

Planetary and Space Science, Volume 237, November 2023, Article number 105778
DOI:10.1016/j.pss.2023.105778

Granular Sample Collection Simulation via Counter Rotating Wheels Sampler for Small-Sized System at Reduced Gravity Environment

E. Sitepu[ab], D. Cullen[b]
[a] Industrial Engineering Department, BINUS Graduate Program – Master of Industrial Engineering, Bina Nusantara University, Jakarta, Indonesia, 11480
[b] School of Aerospace, Transport and Manufacturing, Cranfield University, College Road, Cranfield, Bedfordshire, MK430AL, United Kingdom

Highlights

- Introduces a set of Archimedes screw feature to a conventional counter rotating wheel (Brush Wheel Sampler).
- Numerical Simulations (Discrete Element Modelling) on granular behaviour interaction to a sample acquisition system on asteroids (microgravity) and other planetary bodies.
- The addition of Archimedes screw at the paddles increases the sampling rate by 48.7% (from 12g to 17.8g sample collection)
- Quick sample collection (< 3s)
- 1U size (CubeSat compatible) sample acquisition system.

Abstract
The launching and planning of space missions for asteroid exploration have increased due to their scientific interest and potential resources for future use, such as composition analysis and In-Situ Resource Utilisation (ISRU) demonstration. Furthermore, the design of sample acquisition systems has been limited to accommodate CubeSats or small-sized payloads, as the utilization of CubeSats for scientific missions is also on the rise. Therefore, sample collection is a critical step in preparing for these missions. The focus of this study is to analyse a conventional counter rotating wheels sample acquisition concept on a granular bed in microgravity conditions on an asteroid, as well as on the Moon and Mars with different gravitational forces. The study introduces a set of Archimedes screws into the wheels as a novel sample acquisition approach and utilizes Discrete Element Modelling (DEM) to analyse it. The simulation shows that the addition of an Archimedes screw sampler is more efficient in collecting samples in a short sampling time (<2 seconds) than a conventional counter rotating wheels. For implementation on planetary bodies with significant gravitational force, such as the Moon or Mars, a limitation is observed and redesigning the sample collection chamber might be necessary to capture the particles. Finally, the study highlights potential future work that could provide a more detailed and comprehensive understanding of the newly designed counter rotating wheels sampler.

Keywords: Sample Acquisition System, *In-situ* Resource Utilisation, Small-sized payload, Microgravity, Granular Behaviour, Counter Rotating Wheels

1 Introduction

Over the past two decades, there has been a significant increase in interest regarding the investigation of the utilization of space resources. The study was initiated in 1964 (Rosenberg, Guter and Miller, 1964). This led to the development of Asteroid Mining concept, a process of extracting valuable metals, with a focus on ISRU on asteroids (Kargel, 1996). Another reason for sample collection is to gain a better understanding of the early solar system and the origin of life. Recently, NASA's OSIRIS-REx spacecraft collected a sample from the surface of the asteroid Bennu on October 20, 2020, using the Touch-And-Go Sample Acquisition Mechanism (TAGSAM) to collect regolith (loose rock and dust) from the asteroid's surface (Walsh *et al.*, 2022).

1.1 Sample Collection Techniques

Several celestial bodies are of significant interest for sample collection missions, with asteroids being one of them. A study suggests that CubeSat landing utilizing pure ballistic descent trajectories could be a feasible option, although it poses significant risks due to limited knowledge of the object's physical characteristics (Gautier et al., 2020). Additionally, asteroids possess the potential to serve as a location for performing ISRU, with an ultralow delta ΔV (Jedicke *et al.*, 2022). Given the increasing possibility of utilizing CubeSats for interplanetary missions (Machuca, Sánchez and Greenland, 2019), the authors suggest the need to investigate the feasibility of a sample acquisition system compatible with CubeSats or small-sized spacecraft that can collect samples from those potential locations, especially asteroids.

Various sample collection methods have been explored, especially for Moon missions (Just *et al.*, 2020). The Brush Wheel Sampler (BWS) is a potential method that employs a pair of counter-rotating wheels fitted with flexible brushes to sweep particles upwards into a collection chamber (Bonitz, 2012). The system is capable of collecting samples from the ground with low complexity, less power requirements, and improved efficiency in reduced gravity environments, such as asteroids. Numerical simulations on various aspects of this technique have been analysed (Schäfer *et al.*, 2017; Wei *et al.*, 2021). Based on various sample acquisition systems, the author suggests that the BWS concept is compatible with small-sized systems and suitable for implementation.

Various space agencies, including NASA and ESA, have developed and tested this concept in reduced gravity environments. The initial test by NASA was conducted in microgravity in 2004, demonstrating the ability to fill sample canisters quickly in just two seconds, as illustrated in Figure 1-1(Bonitz, 2012). However, this technology is limited to loose or soft surface material and may pose difficulties in hard rock sampling implementation.

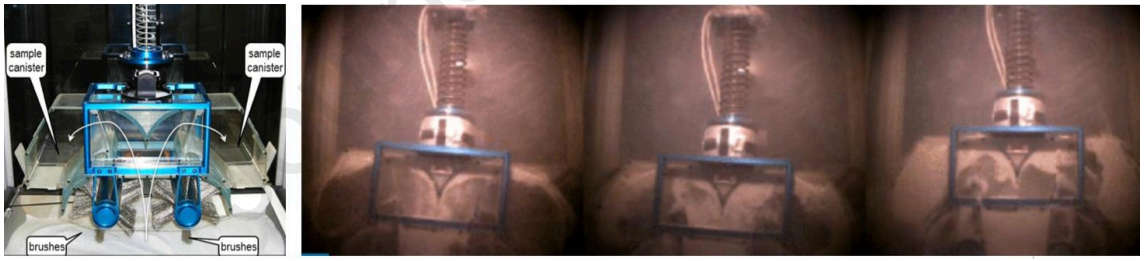

Figure 1-1 (Left) NASA 2nd generation 2-wheel BWS prototype for testing in reduced gravity environment via parabolic flight. (Right) Typical sampling event during testing in reduced gravity, showing the ability to fill sample canister in approximately 2 seconds. Images from (Bonitz, 2012)

Various sampling designs have been tested to improve the sampling efficiency in different conditions. A study tested a 3-wheel BWS design on both flat and 30° sloped surfaces, as depicted in Figure 1-2. The study made three notable observations. Firstly, both the 2-wheel and 3-wheel BWS designs were able to collect a sufficient amount of material in a short amount of time. Secondly, the 3-wheel BWS design outperformed the 2-wheel BWS design, with a higher sampling collection rate of 0.71kg/s compared to 0.47kg/s. Lastly, the 3-wheel BWS design demonstrated greater robustness to surface inclination (Bonitz, 2012). This counter rotating wheel concept for sample collection is then taken as the basis to develop a CubeSat-compatible sample acquisition system for a reduced gravity condition.

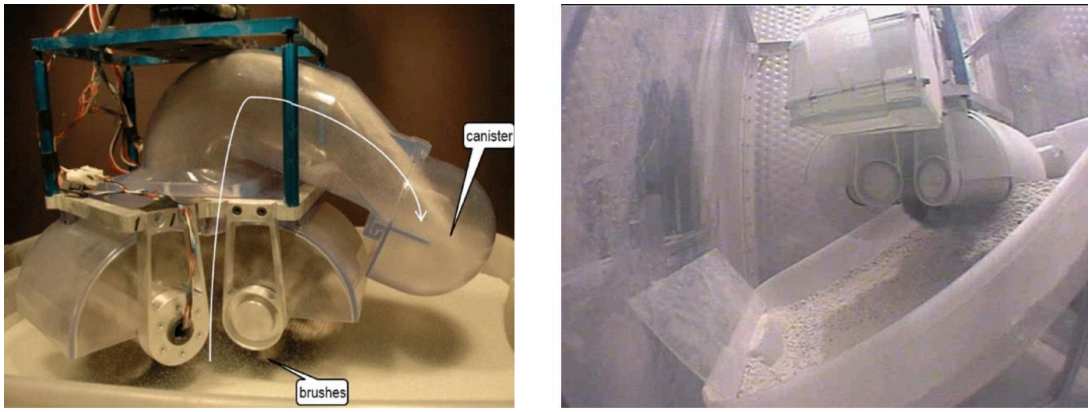

Figure 1-2 (Left) NASA 3-wheel BWS concept of a flat surface. (Right) Demonstration of 3-wheel BWS on surface condition with 30° slope. Images from (Bonitz, 2012)

1.2 Mission Concept

The objective of this study is to develop a miniaturized sample acquisition system suitable for a Cubesat mission scenario, as illustrated in Figure 1-3. The proposed Cubesat mission concept aims to demonstrate sample collection capabilities for an early In-Situ Resource Utilization (ISRU) demonstration. The envisaged approach involves integrating the sample acquisition system within a 6U CubeSat, with dimensions of 20 cm x 10 cm x 30 cm. Adjacent to the sample acquisition system, the ISRU module (e.g., Water Extraction + Electrolysis Module) is positioned to facilitate the heating of the collected sample within a heated cylindrical oven/chamber.

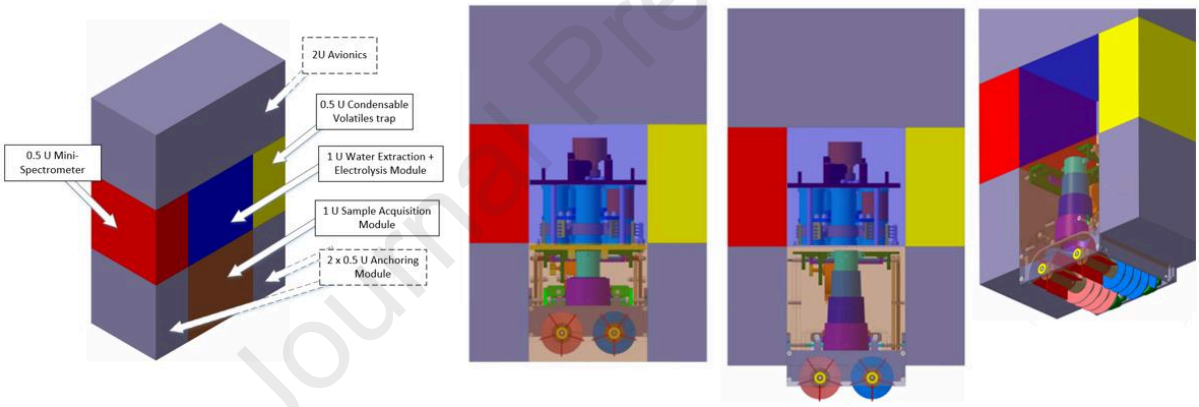

Figure 1-3 CAD representative of a 6U CubeSat concept and the internal system.

Figure 1-4 provides an illustration of the proposed design for a flight model. The Archimedes screw is anticipated to enable lateral transport of regolith from the far side to the paddles mounted under the funnel. The Archimedes screw may be made of flexible bristles to ensure low contact force.

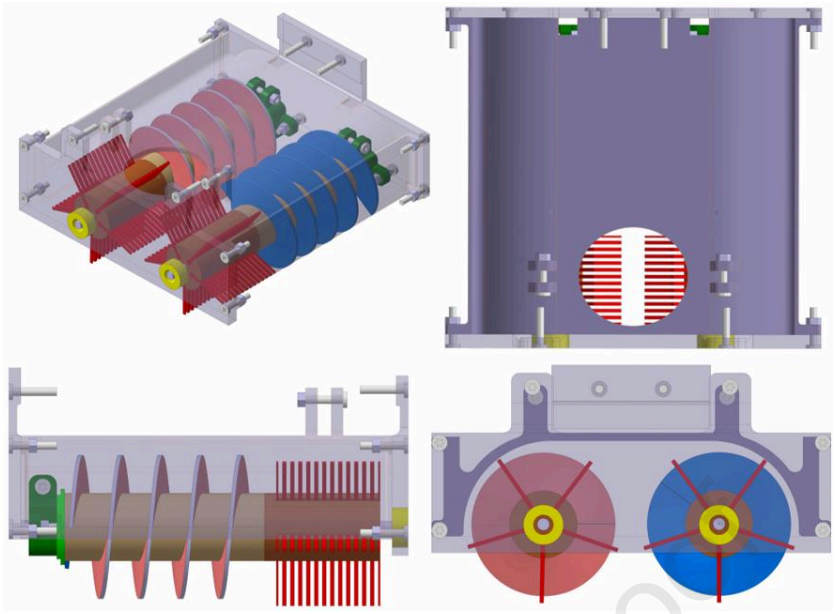

Figure 1-4 Flight model – Sampler. (Top Left) Back 3D view with transparent top, front and back case. (Top Right) Top view with non-transparent top case. (Bottom Left) Side view with transparent side case. (Bottom Right) Front view with transparent front and back case. Note that the Archimedes screw should be composed of brushes. However, for visualisation purposes, it is displayed as a solid structure.

This paper will provide a comprehensive account of the design process for the sampler, and its conformity with the design assumptions. The author will employ discrete element modelling to assess how modifications to the physical structure of the sampler affect its sampling performance. Furthermore, the behaviour of particle sampling in other planetary bodies, including the Moon and Mars, will also be investigated.

The primary assumption underlying this study is that the CubeSat or sampling system has securely landed and become affixed to the ground, thereby constraining the mobility of the spacecraft. Moreover, the sample acquisition system has been devised to transport particles/samples to a collection of chambers through a funnel, as demonstrated in Figure 1-5. With regards to the design requirements, it is directed that the sampler occupies a 1U CubeSat volume, measuring 10cm x 10cm x 10cm.

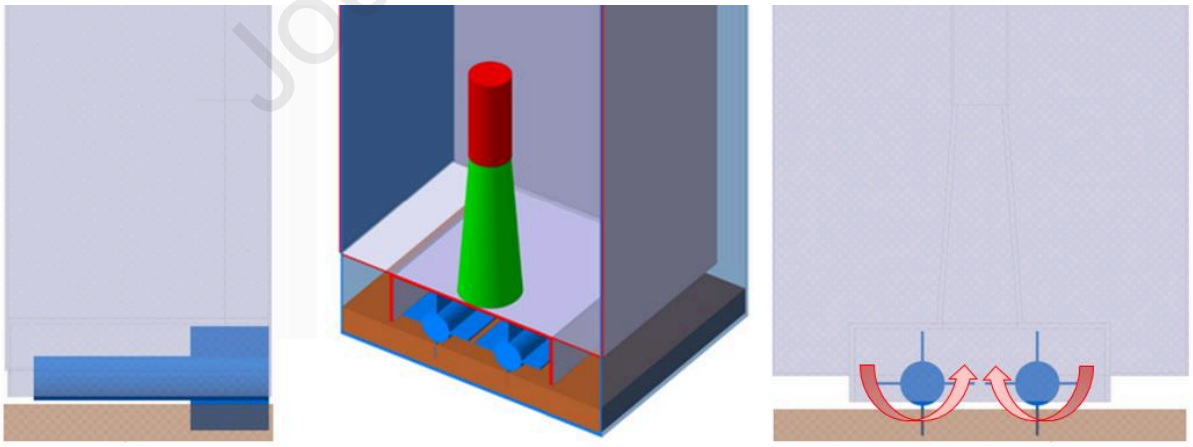

Figure 1-5 CAD representative of simplified sample acquisition geometry without Archimedes screw. (Left), side view. (Middle), sliced 3D view. (Right), front view. Blue: Counter rotating wheels. Green: Funnel. Red: Chamber. Grey: CubeSat volume. Brown: regolith bed (the thickness will be varied). The diameter of the wheel (including the length of the paddle) is 40mm.

2 Objectives & Sample Acquisition Simplified Design

The aim of this investigation is to explore the optimal design for a sampler that can efficiently gather regolith from beneath the funnel, while simultaneously maximizing the sampling capabilities across the entire area of the sampler's footprint.

In pursuit of this objective, three distinct design alternatives have been developed. The first design incorporates the original configuration, depicted in the top-left panel of Figure 2-1. This simulation aim to understand the base performance of sample collection.

The second design involves the extension of the paddles, as demonstrated in the top-right panel of Figure 2-1. This simulation aim not only to see the optimum performance of a standard paddle but also as a comparison to the sampler with Archimedes screws.

The third design integrates a pair of Archimedes screws, that rotates on the same axis as the counter-rotating paddles, as illustrated in the bottom panel of Figure 2-1. The aim of this simulation is to observe/test if the addition of Archimedes screws able to increase the sample collected in the oven/chamber.

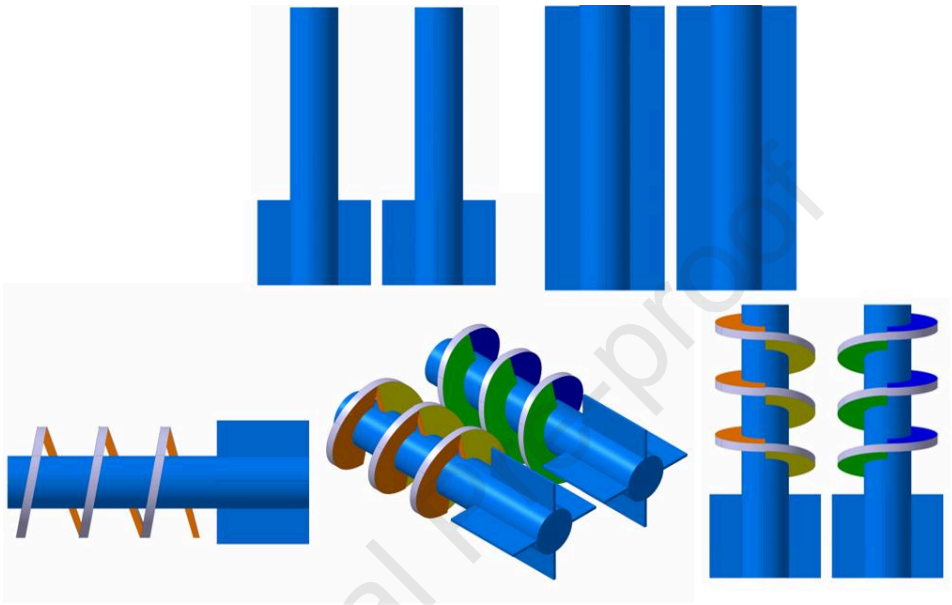

Figure 2-1 Three sampler geometry set-ups. (Top Left) Top down view Standard counter rotating wheels with standard paddles with 26mm in length. (Top Right) Top down view with extended-width paddle with 100mm in length. (Bottom) Combination of Standard paddle + simplified Archimedes screw, viewed from the side, isometric and top down.

3 Simulation Plan and Hypothesis

The primary objective is to determine the sampling attributes of samplers with different designs. The hypothesis predicts that incorporating the Archimedes Screw feature into the sampler will enhance its sample collection rate by providing more material to the paddles. The paddles are designed to transport the in-situ material vertically to the chamber, while the Archimedes screw is proposed to supply material to the paddles horizontally. In essence, the Archimedes screw is anticipated to supply material to the paddles, which in turn will supply material to the oven/chamber.

This section aims to establish a comprehensive test plan to characterize the proposed concept's performance in simulated microgravity conditions for asteroid implementation. Furthermore, the test plan will evaluate the feasibility of implementing the concept in other locations, such as the Moon and Mars, as these locations are currently the most promising sites for in-situ resource utilization (ISRU) and sample collection missions.

Prior to conducting a full-scale size sampling simulation, the author conducted a simplified model simulation. This approach provides preliminary indications of the expected performance in significantly less simulation time compared to a full-sized simulation. Performing a full-sized simulation is computationally intensive and may take several days to complete, even with the use of a High Performance Computer (HPC).

Based on the particle flow presented in Figure 3-1, it appears that the chamber/oven in the simulation code SC (sampling with Archimedes screw) is more densely populated than in VC (sampling without Archimedes screw), as evidenced by the cylindrical shape highlighted in red. It is worth noting that both images were captured at identical times and rotation speeds. A conspicuous observation is the dearth of particles observed at the far side (back) in SC compared to VC. This observation indicates that the design of the pseudo-Archimedes screw (simplified geometry) is effective in its intended task of supplying particles from the far side (back) to the sampling

area (paddle). In conclusion, this simplified simulation suggests that the pseudo-Archimedes screw design/geometry is functioning as intended and provides benefits in terms of sample collection.

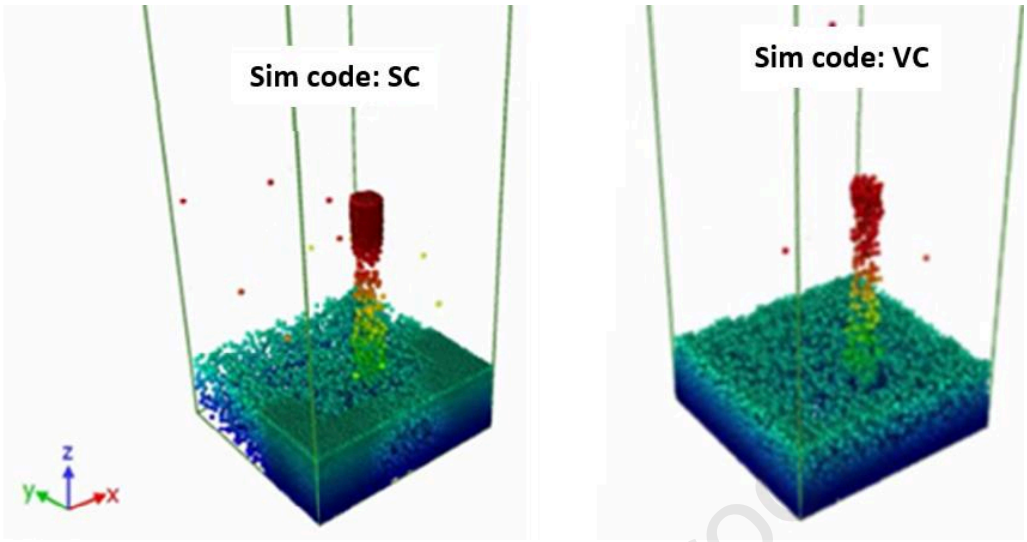

Figure 3-1 A simplified simulations shows particle flow comparison between VC, simulation without pseudo-Archimedes screw and SC, simulation with pseudo-Archimedes screw. Both are at identical rotation speeds and sampling times. Colours are representing the height in the z-axis of each particle. Those coloured red are when the grains' height is above the insertion port of the oven. The paddle and Archimedes screw are located along the y-axis.

The full-sized model includes more particles and a larger simulation box, which then produce higher fidelity in order to mimic asteroid sampling implementation. Currently, three distinct types of tests have been conducted to ascertain the sampling characteristics of the concept. Table 3-1 provides a summary of the proposed test plan for characterizing the sample acquisition concept.

Table 3-1 Brief summary of test plan to characterise the sample acquisition concept with a full-sized model.

	Test Plan	**Aim**	**Variables**
1.1	Sampling of various sampler types	To recognise the actual sampling performance increase with the Archimedes screw and increase assurance of its advantage	Sampler geometry. Standard paddle, standard paddle+ Archimedes screw, Extra width/extended paddle
1.2	Sampling under failure mode	To recognise the decreasing performance relationship to rotation speed	One set of paddle-Archimedes screw at 0rpm at various rotation speeds
1.3	Sampling at other potential ISRU locations	To observe the compatibility of the sampler with other bodies, such as Mars, Moon and Earth	Value of surface gravity

4 Simulation Set-up

In this section, methodologies are presented for conducting numerical simulations that closely replicate actual sampling procedures on asteroids. Specifically, Discrete Element Modelling will be employed to simulate particle flow through the utilization of LAMMPS (Large-scale Atomic/Molecular Massively Parallel Simulator), an open-source software. Open Visualization Tool (OVITO) will be utilized to visualize and measure the particles collected within the chamber.

One crucial feature from the potential numerical simulation tool is to be able to adjust or modify the value of gravitational force. Another important feature is to simulate particle to particle and particle to surface interaction, for instance the friction and rebound. LAMMPS is able to compute or simulate the required features, although there are several limitations. Note that the simulation in this work utilised the February 2020 LAMMPS version.

4.1 Granular Parameters and Baseline Set-up

This section aims to achieve two primary objectives. Firstly, to establish the baseline values for the contact properties between particle-particles and particle-wall geometry. Secondly, to design and construct a representative setup that accurately simulates actual sampling conditions.

4.1.1 Particle-Particle Contact Properties

In this simulation, the mechanical and physical properties of a particle are the most significant factors. At this early stage of sampling characterization, chemical or thermal properties are not mandatory. The necessary mechanical properties for input include grain density, Young's Modulus, and Poisson's ratio. Additionally, the physical aspect, such as the grain size, is required. This section provides an overview of the process for selecting the necessary grain properties and the resulting values for use as input in the simulation. Table 4-1 presents the summary of the assumed values for particle-particle contact properties.

In this simulation, the size of the grain is the only adjustable physical property. Research indicates that small celestial bodies (with a diameter of less than approximately 20km and surface gravity less than 1 x 10-2m/s^2) are covered by relatively coarse regolith grains with particle sizes typically ranging from millimeters to centimeters (Gundlach and Blum, 2013). On the other hand, large objects (with a diameter greater than approximately 80km and surface gravity greater than 6 x 10-2m/s^2) possess very fine regolith with grain sizes ranging from 10μm to 100μm (Gundlach and Blum, 2013). Another study estimates that the grain sizes of the C-type asteroid Ryugu are between 1 and 10mm (Müller *et al.*, 2017).

The current design of the insertion port at the sample canister/chamber has a diameter of 20mm, necessitating that the particle size be less than 20mm to fit inside the oven volume. Initially, the plan was to evaluate the collection rate of the design using a combination of particle distributions, including a monodisperse distribution ranging from 1mm to 10mm, as well as a polydisperse distribution comprising two and three different diameters. However, due to time constraints, the most practical approach was to use a single size of monodisperse distribution. Initially, a grain size of 1mm was used, but the number of particles required to construct a certain regolith thickness was relatively excessive, necessitating a longer computational time, as described in Section 4.4. Consequently, a simulation using 2mm grain size was performed. This setup required half the total number of grains used in the previous simulation with a 1mm diameter, thereby reducing the computational load. The 2mm grain size was ultimately selected for all simulations as an initial research and characterization, as the simulation can be completed within 3-5 days of running time.

Regarding the mechanical properties of particle-particle interaction, the grain density value used is derived from the predicted values for CM and CI Chondrites, which are 2.96 ± 0.04g/cm^3 and 2.42g/cm^3, respectively (Macke, Consolmagno and Britt, 2011). Initially, the plan was to investigate the sampling performance on various grain densities, ranging from the lower density of 2.42g/cm^3 to the higher density of 2.96g/cm^3. However, due to time constraints, these studies have been identified as a future research plan. To initiate early research, the selected density is the average of the lower and higher density values, which is approximately 2.69g/cm^3.

Young's Modulus of Elasticity is an essential input for the mechanical properties. Various chondrites are commonly used to determine the properties of an asteroid, including Young's Modulus of Elasticity. The mechanical properties of different chondrites, such as ordinary, carbonaceous, L, LL, and H, are summarized by Flynn and the values of Young's Modulus of Elasticity vary between nearly zero and 140GPa (Flynn *et al.*, 2018). For wet carbonaceous chondrites, based on 27 carbonaceous samples, the Young's Modulus of Elasticity is reported to be 11.8 ± 1.8GPa, while for dry carbonaceous chondrites, it is 18.9 ± 3.7GPa (Ibrahim, 2012). Therefore, the initial testing value is set to the lowest predicted value of 10GPa, which is obtained from wet carbonaceous chondrites. It should be noted that the ISRU payload study is primarily targeted at a C-type asteroid. This value corresponds to a typical Young's Modulus of Elasticity of loose sand.

The Poisson Ratio is another crucial input for the mechanical properties. As the selected value of Young's Modulus of Elasticity is similar to that of loose sand, the Poisson Ratio value for this simulation will also be obtained from the properties of loose sand, given the limited information available. The Poisson Ratio value for loose sand typically falls within the range of 0.15 to 0.4. For this initial research stage, a value of 0.3 is used, which is the approximate average of the lower and upper limit values.

Two additional parameters are the particle distribution and shape. Although this variation are not performed in this study, it is clear that these parameters may influence the sampling performance. In this preliminary investigation, the assumption was made that the particles have a monodisperse distribution and a spherical shape.

Table 4-1 Assumed grain mechanical-physical properties for particle-particle contact parameter.

Paramater	Assumed Properties	Loose Sand	CM Chondrites
Grain Density (g/cm^3)	2.6	1.62	2.96 ± 0.04
Grain Young's Modulus (GPa)	10	10.35 – 24.15	18.9 ± 3.7
Poisson Ratio	0.3	0.15 to 0.4	-
Particle Size Diameter (mm)	2	0.05 - 2	300µm
Particle distribution	Monodisperse	Polydisperse	Polydisperse
Particle shape	Spherical	Angular to Spherical	-

4.1.2 Particle-Wall Contact Properties

The present sampling simulation is influenced by the particle interaction and the design of the sampler apparatus, including the paddles, Archimedes screw, sampler cover, funnel, and internal oven. While the material of the sampler apparatus is yet to be determined in this research, the common assumption for space applications is that metallic materials such as steel and aluminium are used. Therefore, in this initial test, steel is presumed to be the material utilized to construct the geometry/wall in the simulation.

In the context of particle-wall contact properties for the simulation, the coefficient of friction and the coefficient of restitution are two critical parameters. For this study, due to time constraints, a single value will be used for each parameter in all simulations. Specifically, the coefficient of friction will be assumed to be 0.30, which is the value for clean sand on a steel plate. Additionally, the coefficient of restitution will be assumed to be 0.68, which is the value for the interaction between Leighton Buzzard Sand on a stainless steel plate (Sandeep *et al.*, 2019).

4.1.3 Baseline Design/Set-up

This section outlines the initial setup for the simulation, beginning with the assumption of the gravity value, determination of the number of paddles utilized, and selection of the geometry for the simulation.

The gravitational value is a constant parameter in this experiment, and for this model, a microgravity value of 0.00009m/s2 is selected. This value is consistent with the expected surface gravity of asteroid Bennu, which is the target of the current sample return mission by OSIRIS-REx (Barnouin *et al.*, 2019).

Another important constant parameter is the geometry of the sampling mechanism that has interaction with the particles, which consists of the sampler (Counter rotating wheels, top and surrounding cover), funnel, and the internal sample canister/chamber. Figure 1-5 displays the constructed geometry in LAMMPS represented by a 3D CAD drawing for an initial set-up. In this early characterisation, four paddles are attached to each wheel. As a result, the Archimedes screw design is simplified for this simulation. The simplification is described in the following paragraph.

The simplified design comprises tilted half-discs with a diameter of 4cm and a 1.2cm gap between their centers, as depicted in Figure 2-1 (bottom). The thickness of each half-disc is set at 0.1cm, and there are a total of twelve tilted half-discs grouped into two sets. The first set, rotating counter-clockwise, has its half-disc centers located at positions of -1.16cm, 1.24cm, and 3.64cm along the y-axis, while the second set, rotating clockwise, has its centers at positions of 0.04cm, 2.44cm, and 4.84cm. The tilt angle is approximately 22.5°, and for the counter-clockwise paddle-Archimedes screw, the first set of half-discs are negatively tilted at the local x-axis (-22.5°), while the second set of half-discs are positively tilted at the local x-axis (+22.5°). The local x-y-z-axis of each half-disc is located at the center of the half-disc. For the clockwise paddle-Archimedes screw, the first set of half-discs are negatively tilted at the local x-axis (+22.5°), while the second set of half-discs are positively tilted at the local x-axis (-22.5°). This counter-rotating wheels geometry, comprising paddles and an Archimedes screw, is utilized for all subsequent tests, except those exploring the impact of sampler types.

In addition to the geometry of the sample acquisition, the size of the simulation box plays a critical role. The objective is to configure the box such that its impact on the particle flow, in terms of the simulation box's geometry or wall, is insignificant.

The first set-up is represented in CAD image in Figure 4-1, first from the left. The sides are 10cm x 10cm (from x = -5cm to x = +5cm and from y = -5cm to y = +5cm) and the height is varied to produce various regolith thicknesses. The rest of the images in Figure 4-1 are the results from LAMMPS, visualised by OVITO. The results from the first height iteration (regolith thickness of 3cm) are shown by the particles (coloured purple) and

show that grains interact greatly with the bottom wall of the simulation box. Therefore, several iterations were needed to define the optimum regolith bed thickness. Note that after increasing the depth to 9.5cm, the first image from the right in Figure 4-1 (yellow particles) seems to minimise its effect over a similar sampling time (10s of sampling). Therefore, a regolith thickness of 9.5cm is selected for the final set-up.

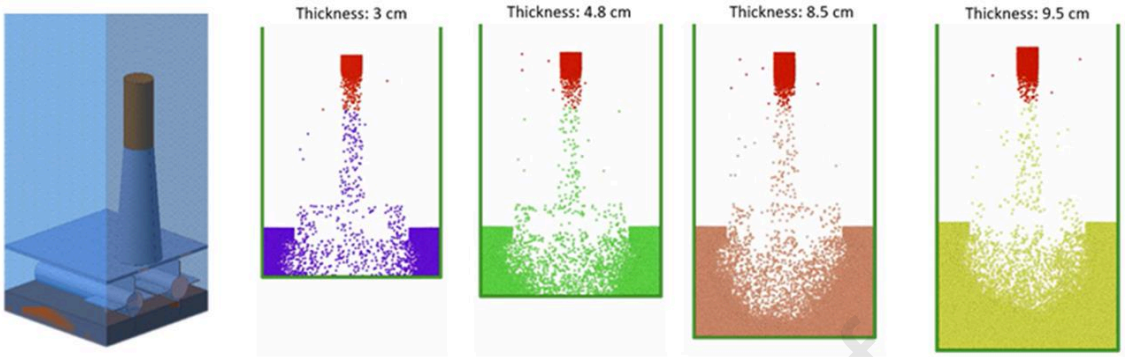

Figure 4-1 (Left), Initial set-up. (Rest of images), Results from LAMMPS, visualised by OVITO, which is the iteration process of increasing the regolith thickness. Results are viewed from x-z-axis. Particles in red indicate that particles are in the volume of the oven.

The grain flow depicted in the right corner of the image appears to remain unaffected by the wall of the simulation box. Nevertheless, this representation fails to accurately emulate a sampling event. In the present configuration, the particle movement is constrained by the side wall, bottom wall, and sampler cover, resulting in a consistent particle inflow to the sampler. However, the actual sampling scenario on an asteroid involves an empty space that is free from obstruction above the surface and on the sides. To achieve a more realistic simulation, the width of the simulation box in the x-y direction must be adjusted.

Several iterations were conducted to optimize the dimensions of the simulation box along the x-y direction. By increasing the length of the sides, the upper limit of the computational load was maximized, with a final setup of 34cm x 34cm as illustrated in Figure 4-2. The utilization of high-performance computing allows for a runtime of 60 to 120 hours (three to five days) to simulate each test plan.

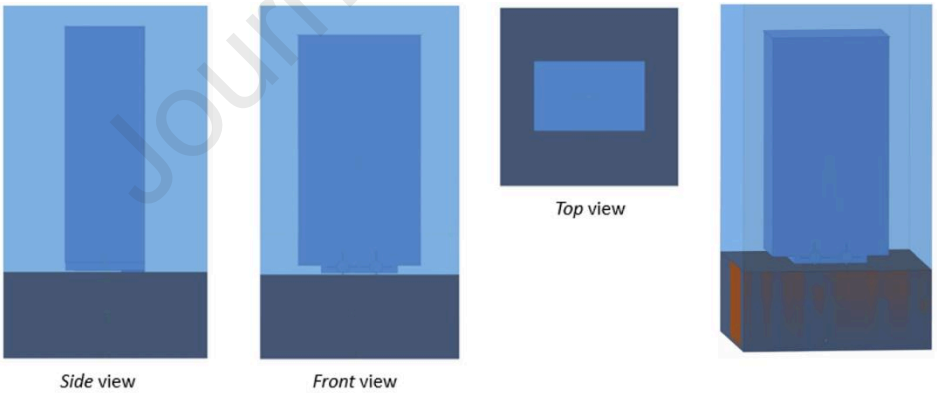

Figure 4-2 Final set-up for sampling simulation. Images are represented in CAD. The sides of the simulation box are 34cm x 34cm (from -17cm to +17cm at the x-axis, from -17cm to +17cm at the y-axis). The height is from -9cm to 100cm (total 109 cm) at the z-axis.

4.2 Simulation Steps

The simulation of the sampling (counter rotating wheels) process involves two initial stages. The first stage involves filling the simulation box (34cm x 34cm x 109cm) with particles. To achieve a 9cm thickness of regolith, a total of 3,813,124 particles were inserted. This first stage, which entails pouring particles, has a duration of 15 seconds, with an additional 5 seconds allocated to ensure that all particles are relaxed. Notably, the simulation time step is set to 0.00001s.

In the second stage of the simulation, the sampler/geometry is introduced into the simulation box, causing the particles to move randomly and instantaneously come into contact with the geometry, such as the lower end of the paddles and the Archimedes screw. Consequently, a waiting period is necessary to allow the particles to settle

back onto the surface and fully relax. To expedite this process, the gravity is increased. To determine the optimal time step, multiple iterations were conducted to establish the minimum or most efficient running time for this stage. The duration of the second stage, which encompasses geometry insertion and particle bed relaxation, is set at 15s.

Upon completion of the relaxation process of the regolith bed, the sampling phase, which involves the rotation of the counter-rotating wheels, may begin. The prescribed duration for this phase is within the range of 15s to 30s.

4.3 Sampling Performance Data Acquisition

To analyse its sampling performance, this project will measure the number of grains trapped in the internal oven chamber throughout the sampling time. This is done by slicing the simulation using the visualisation software (OVITO), thus being able to focus only on the grains in the chamber, as seen in the bottom right image of Figure 4-3. This is necessary since it is not feasible to observe the oven without slicing, as presented in the left top image of Figure 4-3.

The slicing requires three steps in order to observe the number of particles solely in the internal oven chamber, as seen on the bottom right image in Figure 4-3. The first slice is at a distance of -3.5cm along the y-axis with a slice width of 2.7cm; 2.7cm is roughly equivalent to the width of the paddle. The second slice is at a distance of 0cm along the x-axis with a slice width of 2.1cm; 2.1cm is roughly equivalent to the diameter of the oven. The third slice is at a distance of +16.12cm along the z-axis, with a slice width of 5.2cm; 5.2cm is roughly equivalent to the height of the oven. Note that the sampler footprint/area is at 0cm on the z-axis from x = -5cm to x = +5cm and from y = -5cm to y = +5cm. By combining the three slices, an image as shown in the bottom right of Figure 4-3 will be seen.

Each frame shows the number of particles at the bottom left corner. For example, the top right image consists of 111,566 particles while the bottom right image consists of 1,222 particles. Note that these images are at a similar time step.

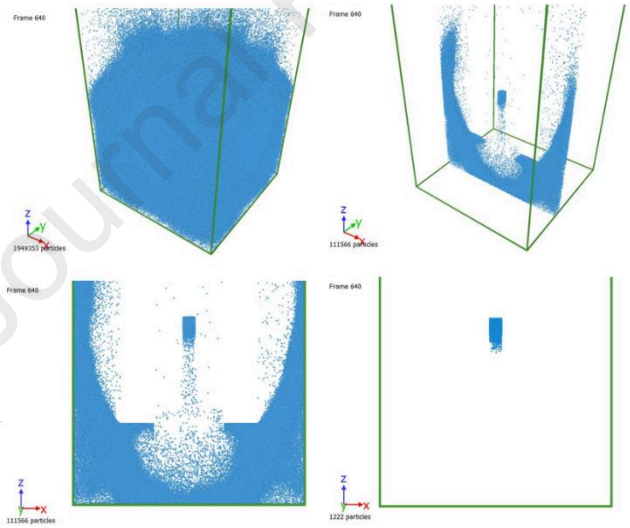

Figure 4-3 Particle flow as seen in OVITO. (Left top) Not sliced. (Right top) Sliced. (Left bottom) Sliced viewed from x-z-axis with thickness of 2.7cm at y = -3.5cm (this view is mainly used for visualisation purposes, the length in x-axis is 34cm from x = -17cm to x = +17cm). (Right bottom) Final slice for data acquisition. Each frame shows the number of particles at the bottom left corner. This number of particles is collected for data acquisition. For example, there are 1,222 particles in the right bottom image.

To observe its upper limit of grain collection capability of 2mm grain diameter in the oven cylindrical volume, a simulation was performed which showed that a maximum of 2,050 particles (spheres) can be trapped in the oven. The number is equivalent to 22.3g. If translated to oven volume, it fills 54% of the cylindrical volume of 10mm radius and 50mm height. This number is sensible, and is slightly lower than the theoretical random sphere packing of 64% due to the void (Scott and Kilgour, 1969). Later, to observe the sampling performance, the total number of particles collected will be compared to the maximum particles' packing capacity (100% "Oven/chamber filled" is equivalent to 22.3g). The term "Oven/chamber filled" will be used as the common method to measure the sampling performance of each simulation.

4.4 Test Limitation

One essential prerequisite for conducting the simulation is the utilization of a high-performance computing system of 128 CPUs with limited running time. This limitation in the maximum computing quota poses an apparent constraint in replicating a realistic sampling phenomenon on an asteroid. One direct implication to this quota is the volume of simulation box, number of particles, number of run for each simulation.

The first limitation was the selection of grain morphology. The available option was to simulate fully spherical grain. Therefore, studying the effect of grain morphology such as sharp edges, or elongated grains is not yet possible. Another limitation is related to the grain to wall/geometry interaction. Based on the manual instruction and description on the LAMMPS webpage, the rebound or resultant reaction force from interaction between particles and the convex surface often produces inaccuracies, which cause particles to escape the simulation box (LAMMPS, 2020).

Due to time constraints, the data collected for each simulation was obtained from a single run. In the future, it is recommended to conduct multiple runs for each simulation to observe any potential variations.

5 Implementation, Results and Analysis of Simulations

In this preliminary investigation of sampling characterization, three simulations were examined. Firstly, an analysis was conducted to evaluate the efficacy or efficiency of incorporating the Archimedes screw. Secondly, an assessment was carried out to examine the sampling performance during failure mode (i.e., one wheel with zero rotation). Thirdly, a series of simulations were performed to observe the sampling performance at various potential In-Situ Resource Utilization (ISRU) sites, including the Moon and Mars, as well as the Earth, to enable comparative analysis.

5.1 Sampling Characterisation using Various Sampler Types

The purpose of this set of tests is to conduct a characterization of the potential sampling advantages obtained by utilizing a pseudo-Archimedes screw. To further enhance the reliability of the results, a different type of sampler is simulated. Specifically, this sampler is an elongated paddle with a y-axis width of 100mm that spans from the front, where the funnel and oven are situated, to the back of the CubeSat footprint.

5.1.1 Test Implementation

The three sampler geometries are presented in Figure 2-1. All other parameters are similar, for instance, the paddle depth to regolith is similar at 9mm. A brief summary of the simulations is presented in Table 5-1.

In this set of simulations, the rotation speed is set at 100rpm. This number is taken as it is predicted to be sufficient to transfer the particles to the oven in a reasonable amount of time (in order of seconds).

Table 5-1 Various sampler type as variable and simulation code.

	Simulation		
Sampler Type	Standard paddle (26mm width)	Standard Paddle (26mm width) + Archimedes screw	Extra width paddle (100mm width)

5.1.2 Test Results

An example of the sampling sequence is presented in Figure 5-1. The images at the top display particles flow at 0s, 0.5s, and 1s for simulation with a sampler that contain a standard paddle (26mm width) and pseudo-Archimedes screw, and the images at the bottom display particles at t = 1s for each sampler type.

The top images in Figure 5-1 display a sequence of sampling events. The rectangular area in the centre (sampler cover) and the funnel are more populated within 0.5s of sampling, if compared to 1s after sampling. This is an indication that the sampling rate is greater in the earlier period of sampling time. After 1s of sampling (top image – right), the internal oven chamber is packed with particles; slightly more condensed than the internal oven in 0.5s (top image – middle). Another interesting phenomenon is also shown at the side of the CubeSat volume, which displays more particles being swept into the empty space surrounding the CubeSat.

The bottom images in Figure 5-1 display the comparison of particles movement/flow from different sampler types at identical time steps of 1s after sampling. The particles in green represent simulation with a standard paddle only (26mm width without the pseudo-Archimedes screw). The particles in yellow represent simulation with the extended paddle (100mm width). The particles in purple represent simulation with a pseudo-Archimedes screw attached to the standard paddle (26mm width). The particles population in the internal oven chamber between simulations is clearly shown. The population of particles in green is less than both yellow and purple. The different

is relatively significant between green and purple. The population of particles with the pseudo-Archimedes screw seems to be almost double the amount of particles with the standard paddle without the Pseudo-Archimedes screw. The results indicate that the addition of the Archimedes screw can increase the sampling rate and also the sample collection performance.

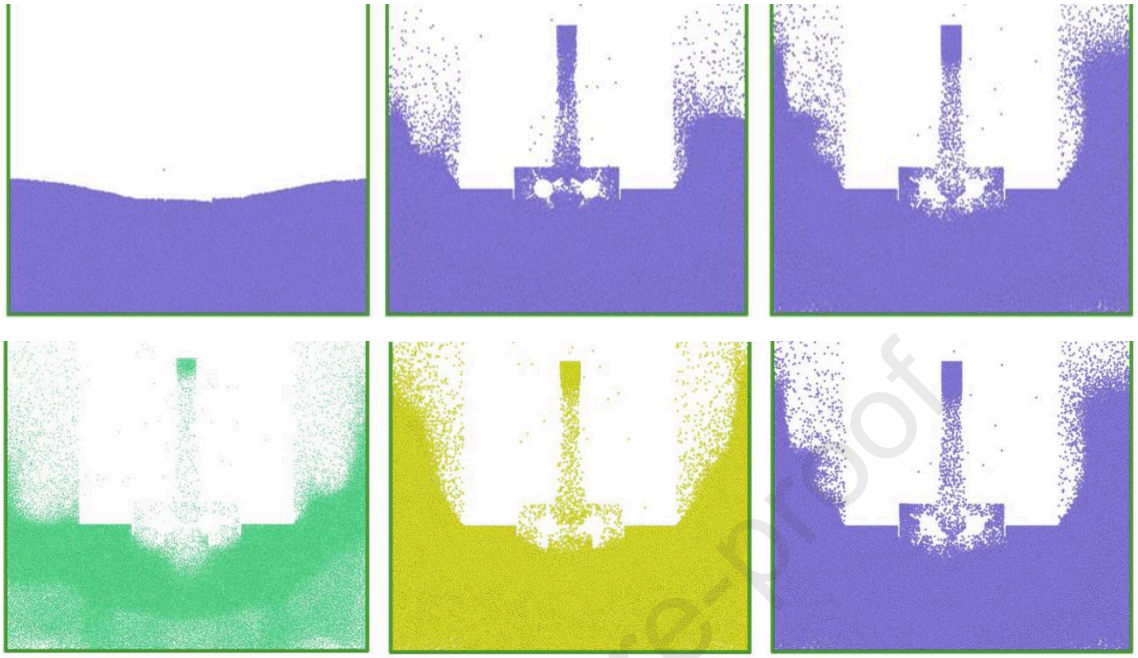

Figure 5-1 (Top) Particles flow sequence for sampler with pseudo-Archimedes screw simulation at 0s, 0.5s, and 1s. (Bottom) Particles flow at t = 1s for each type of sampler. Green – Standard paddles without Archimedes screw. Yellow – Extended width paddles. Purple – Standard paddles plus pseudo-Archimedes screw.

The sample collection throughout the sampling time is presented as a graph in Figure 5-2. The sample collection is valued by the oven filled percentage, which is a comparison between the collected sample and the maximum sphere packing in the oven. Note that the maximum packing (100%) is equivalent to ~22.3g. The graphs show a clearer representation of the benefit of the pseudo-Archimedes screw in sample collection performance. All the simulations show a similar trend with a high sampling rate below 2s of sampling and significantly low sampling rate after the 2s of sampling. The particles population inside the oven chamber either stays there for a period of time or bounces back to the surface, which then decreases the amount of particles in the chamber through time. After 2s of sampling, the sampler with only a standard paddle fills ~54% of maximum oven capacity of packing the 2mm particles size; this number is equivalent to 12g of the sample. However, the sampler with the extended paddle size is able to collect 60% of the sample (~13.4g). For the sampler with the pseudo-Archimedes screw attached to the standard paddle, 2s of sampling is able to fill the oven's capacity to 80% (17.8g of the sample).

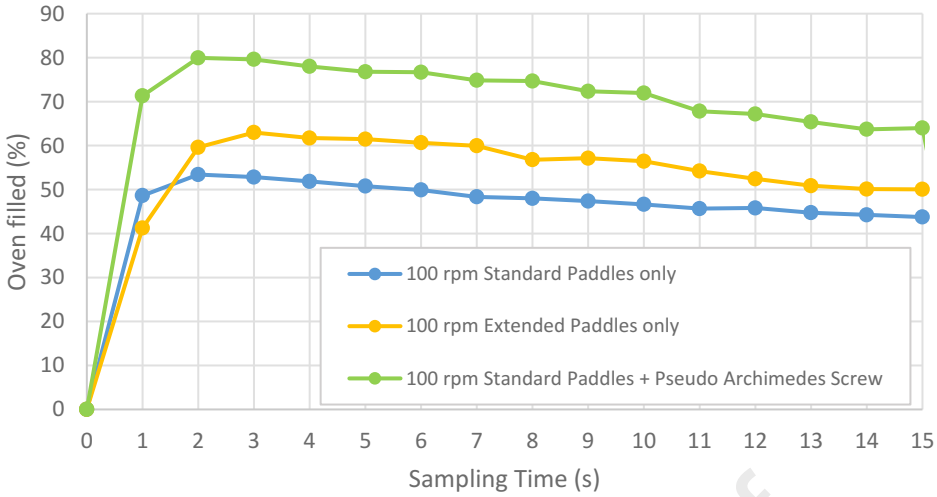

Figure 5-2 Sampling performance comparison between sampler type based on maximum oven capacity.

5.1.3 Test Discussion and Conclusion

The results of sample collection between each sampler type validates that the addition of a pseudo-Archimedes screw is advantageous in terms of sample collection performance. The sample collection could reach 17.8g (~80% oven filled) in under 2s of sampling, while standard and extended width paddles obtain 12g and 13.4g of particles, respectively. After 2 - 3 seconds, the sampling rate declines, as particles underneath the sampling area are reducing, either transported to the oven or swept out into the empty space surrounding the CubeSat.

The increasing number of particles collected by the extended paddle width (from 26mm to 100mm) is only by 11.7% (from 12g to 13.4g). The increasing number of particles collected by the sampler with the pseudo-Archimedes screw compared with that of the sampler with the standard paddle only is a significant 48.7% (from 12g of the sample to 17.8g of the sample). If comparisons are made between the extended width paddle and the standard paddle with the pseudo-Archimedes screw, the sample collected with the latter after 2s of sampling is still significantly greater, as it increases by 33% (from 13.4g to 17.8g of the sample).

To conclude, the study confirmed that implementation of the Archimedes screw feature is advantageous by providing a greater sample collection within a similar sampling time. Therefore, the rest of the simulation will use the paddle plus pseudo-Archimedes screw sampler in the set-up.

5.2 Sampling Characterisation at Failure Mode with the Archimedes Screw

This section characterises the reliability of the sampling concept by performing a failure mode operation. The reliability at this set of simulation is valued by its sample collection performance at failure mode. A failure in this study is defined as the incapability to rotate one set of paddle-Archimedes screws.

There are various cases resulting in a non-rotatable wheel (paddle-Archimedes screw set), and these can be caused by the internal system and/or external issues. For instance, the case caused by internal system error is due to motor failure. Another potential failure is due the failure from the electrical connection to the power supply. While for the external cause, various particles sizes from micron to cm at the actual sampling demonstration at the surface of the asteroid can jam the movement of the paddle-Archimedes screw and/or jam the motor. Therefore, this set of simulations is planned to observe the sampling performance characteristics of this undesirable event.

5.2.1 Test Implementation

For this model, the set-up is to situate one set of paddle-Archimedes screws at 0rpm. To observe the performance comparison, normal/standard operation is set as the baseline. Since the previous simulation used 100rpm at normal mode, then a failure mode at an identical 100rpm is also performed as a comparison. Then, an attempt to restore the initial/normal sampling performance is done by increasing the rotation speed. For an initial iteration, a rotation speed of 200rpm (double the initial rotation speed) is set. A brief summary of simulations are presented in Table 5-2. F1/D2 is the code for standard/normal operation, which has identical data to the previous set of simulations in Table 5-1 that used the pseudo-Archimedes screw.

Table 5-2 Mode of operation and simulation code.

	Simulation code		
Variable	F1/D2 Pseudo Archi.	F2 Pseudo Archi.	F3 Pseudo Archi.
Mode - speed	Normal - 100rpm	Failure - 100rpm	Failure - 200rpm

5.2.2 Test Results

The particles flow between each simulation is presented in Figure 5-3. These images are comparisons between two different modes at similar times of one second after motor rotation initiation. The image on the left is the normal operation mode at 100rpm. It can be seen from the void of particles in the centre (the rectangular granular distribution area) that both paddles from the clockwise and anti-clockwise wheels are rotating. Based on the visualisation, the particles almost populate the entire internal oven chamber. If compared to the image in the middle, which is the failure mode at 100rpm, clearly one of the wheels (anti-clockwise rotation) is not rotating. The volume at the anti-clockwise region is populated with particles (since the particles are not swept from the anti-clockwise paddles and potentially pile up in that region due to the particle movement from the clockwise paddles), while the volume at the clockwise region is filled with fewer particles, due to the particles being swept by the paddles (clockwise wheel). A significant difference is shown in the number of particles inside the internal oven chamber. The population is obviously less than the normal operation mode (100rpm – both wheels rotating). Lastly, the image on the right represents the particles state at 200rpm rotation speed at an identical time step. Here, the number of particles populating the internal oven chamber increases if compared to the 100rpm failure mode simulation. However, it is clearly seen that the number of particles in the internal oven chamber are still fewer than the normal mode of 100rpm rotation speed.

Figure 5-3 Particles flow comparison between various operations at one second of sampling. (Left) Normal/standard 100rpm operation. (Middle) Failure mode at 100rpm. (Right) Failure mode at 200rpm.

The sample collection throughout the sampling time is displayed as a graph in Figure 5-4. The graph only shows the first three seconds of sample collection after the initiation of motor rotation. Thus is able to show the sampling performance more clearly; also the sampling rate decreases after two seconds from motor rotation initiation. The sample collection of a 100rpm rotation speed during failure mode decreases to 24% maximum oven capacity from 70% at normal operation, after one second of motor initiation. By doubling the rotation speed (from 100rpm to 200rpm), the sample collection increases to roughly 32% from the previous 24%.

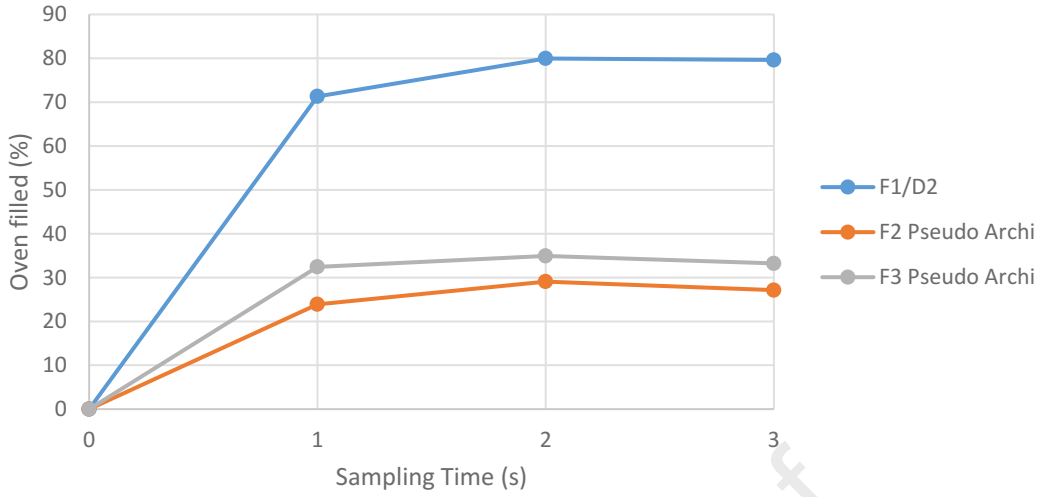

Figure 5-4 Sampling performance comparison between normal and failure operation at 100rpm & 200rpm. F1/D2 is a normal 100rpm sample collection in the internal oven through time. F2 Pseudo Archi is the failure operation of F1/D2. F3 Pseudo Archi is a failure mode at 200rpm.

5.2.3 Test Discussion and Conclusion

The results show that the sampling concept is still able to collect samples during failure operation, although the performance decreases. For instance, 6g (~30% oven filled) are collected rather than the previous 18g (~80% oven filled) at normal operation with two seconds of sampling at a similar rotation speed of 100rpm. Another simulation was done by increasing the speed to 200rpm and was able to collect 8g (~35% oven filled) after two seconds of sampling. This means that sampling performance can be restored at a certain level by increasing the rotation speed. This action is relatively straightforward by merely increasing the power/current supply to the motor. Nonetheless, this action might influence the load of the anchoring mechanism since a higher rotation speed might produce higher vibration, which could disturb the CubeSat stability.

As a conclusion, this set of simulations displays the reliability of the sampling concept although failure occurs by not being able to rotate one wheel of the counter rotating paddle-Archimedes screw.

5.3 Sampling Characterisation at Other Potential ISRU Locations with Archimedes Screw

In this section, a set of simulations is prepared to observe the implementation of the sampling concept at other potential ISRU locations, such Moon/Moon and Mars. A simulation at Earth is also performed as reference. This simulation will display clearly the influence of variation in the gravitational field.

5.3.1 Test Implementation

The tests use an identical set-up with the only difference being the value of surface gravity. The simulation code and its variables (surface gravity value) are presented in Table 5-3. Since most of the previous tests use 100rpm for comparison, therefore for an initial testing, an identical 100rpm rotation speed is selected. For future work, simulation at various speeds might be needed to observe the minimum rotation speed to be able to sweep material from the surface to the internal oven chamber region at different solar system locations, using the sample acquisition design.

Table 5-3 Simulation code for various locations and rotation speeds.

	Simulation code:			
Variable	L1 (Moon)	M1 (Mars)	E1 (Earth)	A1/D2 (Asteroid)
Surface gravity (m/s^2)	1.62	3.71	9.81	0.00009

5.3.2 Test Results

The particles flow between each simulation at 100rpm is presented in Figure 5-5. The figure shows sliced images viewed from the x-z-axis at y = -3.5cm with a width of 2.7cm, at various time steps. The value of gravity is increasing from the top to bottom row, starting with the asteroid (purple particles) with microgravity, Moon (grey particles) with $1.62 m/s^2$, Mars (orange particles) with $3.71 m/s^2$, and comparison to Earth (blue particles) with $9.81 m/s^2$. The time step at each frame is at t = 0s, 0.25s, 0.5s, 0.75s, 1s, 1.5s, and 2s.

At the asteroid implementation, it can be seen that the lack of gravity is helping the sampler to transport the particles from the surface to the internal oven chamber. The particles are also "flying" from the sides of the CubeSat volume to the empty space in the simulation box. If the simulation is not sliced, the particles are seen "flying" around the CubeSat volume; this phenomenon can be seen on the top left image in Figure 4-3. The area (also volume if viewed from the x-y-z-axis) underneath the sampler (paddle-Archimedes screw feature) is also greatly affected by showing a significant particles void (refer to the image at t = 1.5s and 2s). The particles were either swept to the internal chamber or to the surrounding environment. At t = 2s, there is a particle void at the bottom corner of each side of the simulation box; this indicates that the particles movement/flow has started to be influenced by the simulation box.

At the Moon implementation, it can be seen that gravity is starting to have an opposite effect on sample collection, if compared with the application on the asteroid. The particle beds are relatively stable; as seen from t = 0s to t = 2s, there are no particles "flying" around the surrounding CubeSat volume. At this rotation speed of 100rpm, it can be seen at t = 0.75s, that some particles were able to reach the height of the internal oven chamber. However, due to significant gravity and no mechanism/feature/structure to capture the particles, the particles fall down to the surface.

At the Mars implementation, surface gravity produced a similar effect as shown in the Moon implementation. However, at 100rpm rotation speed, there is no indication that the particles were able to reach the height of the oven.

At the Earth implementation, the rotation speed of 100rpm cannot sweep the particles to the height of the funnel. The particles are stirred around the paddle-Archimedes screw geometry.

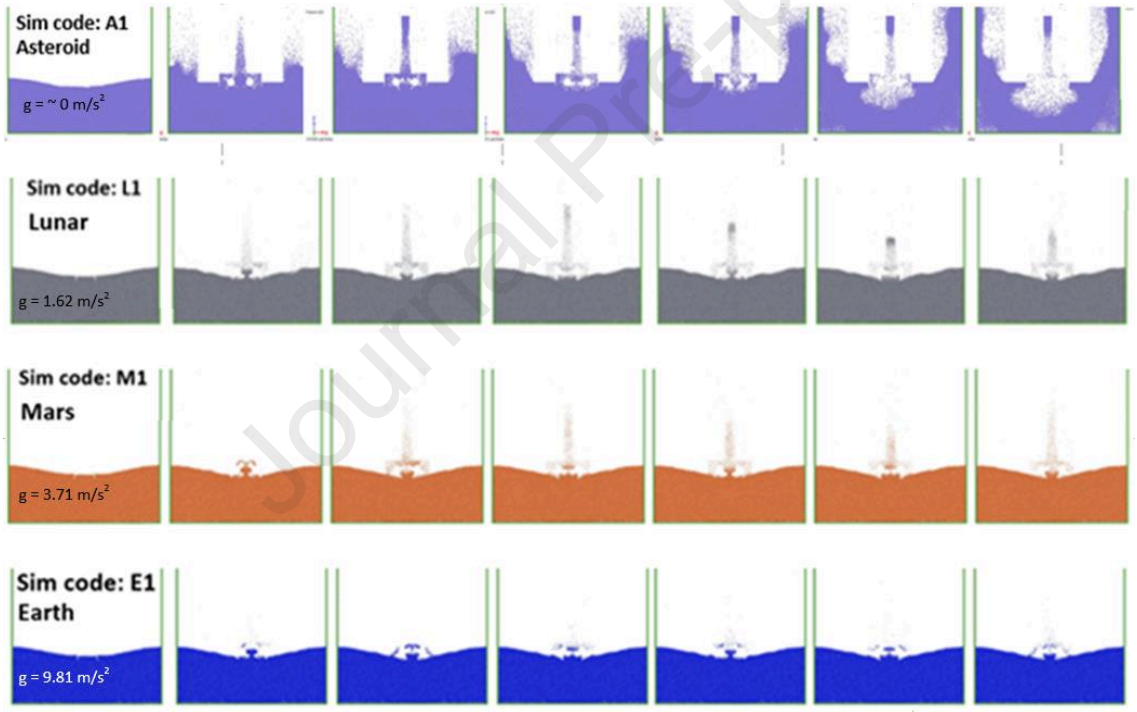

Figure 5-5 Particle flow comparison at various space bodies with 100rpm rotation speed. Sampling time from left to right, t = 0s, 0.25s, 0.5s, 0.75s, 1s, 1.5s, and 2s. Images are sliced and viewed from the x-z-axis.

5.3.3 Test Discussion and Conclusion

This set of testing displays sampling characteristics at other bodies with various gravity values. Results from Figure 5-5 display the phenomenon of sampling at 100rpm on the asteroid, Moon, Mars, and Earth. It clearly shows that no particles are able to stay inside the internal oven chamber for a significant period of time; except for implementation on the asteroid.

Although, at the Moon implementation, several particles are able to reach the internal oven for a period of time in seconds (see Figure 5-5 for L1 at t = 0.75s) before falling back to the surface due to gravity. Some particles are bounced back upwards when they hit the paddle during descent and some particles fall down to the surface. The cycle continues since the Archimedes screw keeps supplying particles to the paddles. A similar phenomenon is also observed on Mars (M1). However, the cycle is quicker since the increased gravitational force reduces the

maximum particles' height and pulls back the particles more quickly. On Earth (E1), the momentum/energy from the rotation speed of 100rpm is not sufficient to transfer the sample from the surface to the height of the oven.

At Moon and/or Mars, if the particles are able to reach the top of the internal oven, this sampling concept might still work in those potential ISRU locations with modifications to internal oven structure or with precision timing during the oven carousel rotation.

The potential modification of the internal structure will be presented in the following paragraph. Regarding precision rotation timing, further simulation is required to quantify the particles' dwell time in the oven, and thus be able to specify how quickly the carousel would need to be rotated. For this project, the time from one indexed oven position to another is not yet defined.

This paragraph proposes a near future research to modify the internal oven structure at those locations (e.g. Moon and Mars) by adding a tilted baffle to capture particles when descending to the surface. The configuration, for instance, number of baffles, tilt angle, thickness of each baffle, and orifice diameter of the baffles, can be varied to optimise the sample collection performance. An example of a modified internal oven in shown in Figure 5-6. The addition of baffles could help the heat transfer to the particles by adding more contact surface-to-particles interaction.

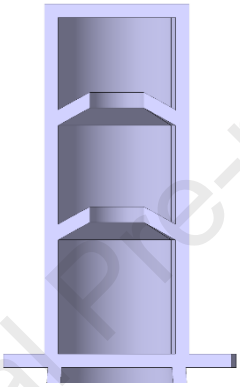

Figure 5-6 Example of proposed internal oven chamber at other space bodies for near future research. Image is sliced at the x-z-axis.

As a conclusion, performing sampling on Moon and Mars might be possible via a counter rotating paddle-Archimedes screw. However, a higher rotation speed (higher momentum/energy) is compulsory and modification to the internal oven might be necessary.

6 Discussion, Summary, and Conclusion

6.1 Discussion

For all simulations, the sampling stage, which starts from the rotation of the sampler lasts for 30 seconds. For implementation on Moon and Mars surfaces, particles interaction that is influenced by the simulation box is minimal. The particles flow beneath the sampling area is still strongly influenced by its grain-grain interaction. In this case, the sampling simulation throughout the complete 30 seconds of sampling is reliable. However, this is in contrast to asteroid implementation. After 1 - 2 seconds of operation, the momentum from the paddles is quickly transferred between grains and reaches the geometry of the simulation box wall; thus influencing the flow of the particles. The sample collection will surely lessen over time, which is sensible, but the accuracy of the simulation will also decline due to higher intervention from the box. Therefore, data collection for the current simulation at an asteroid should only take the first 1 - 3 seconds to have reliable results.

Sampling on an asteroid can be made in less than a few seconds (e.g. a larger simulation box will be needed to specify the actual time needed to reach the sampling rate peak). Afterwards the sampling operation can be stopped if necessary since most of the simulation shows a declining sampling rate as displayed in Figure 6-1. In the current simulation and set-up, sampling within two seconds is sufficient to be able to fill the oven up to 80% of the maximum capacity, for a monodisperse 2mm grain size (diameter). The number is equivalent to a sample collection up to 18g. During failure operation, the sampler is still able to collect around 6 grams (~30% oven filled) at 100rpm, around 8 grams (~35% oven filled) at 200rpm.

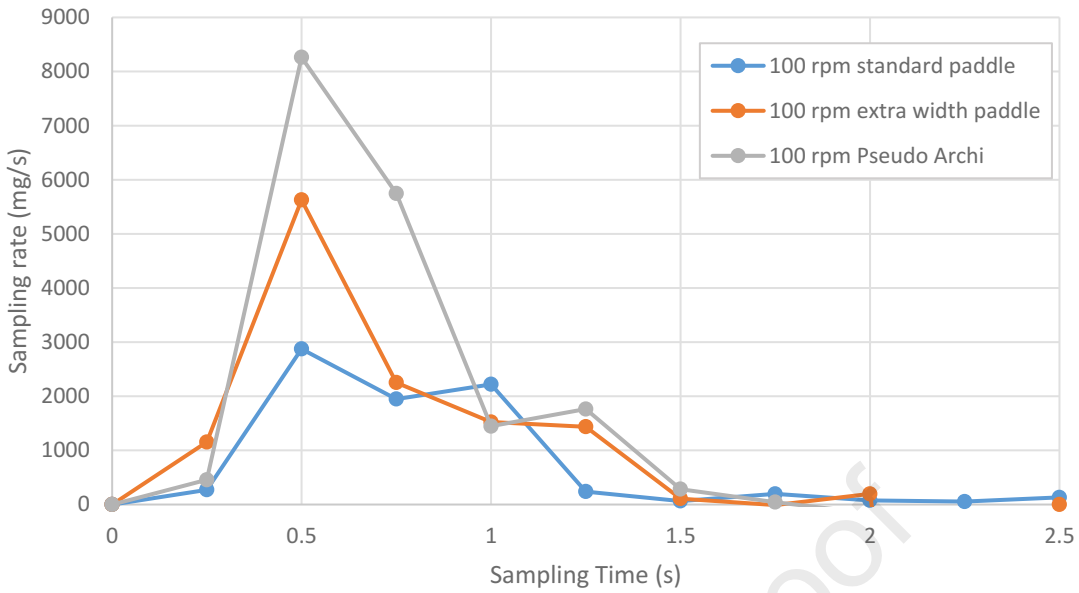

Figure 6-1 Sampling rate on asteroid implementation for monodisperse grain size of 2mm in diameter under various conditions.

For the overall mission, five (four plus one) ovens are prepared. For the requirements, the sampler should provide 12g of *in situ* material for each oven, which means a minimum of 36g should be provided to the three ovens for three demonstrations. Also, if there is a failure during extraction at the first three attempts, the sampler is expected to fill the remaining two ovens, which means another 24g of sample is needed. However, the sample mass requirements is to be updated along the advancement of the project.

Based on the results visualised in Figure 6-2, sampling time shows the crucial role of the availability of particles underneath the sampling region. As seen in Figure 6-2, five seconds of sampling time results in decreasing significantly the number of particles underneath the sampling region. Therefore, the strategy of having an extendable sampler via the scissors mechanism in order to be able to reach a fresh sample is required. However, to observe its efficiency/sample collection performance in higher fidelity, a larger-wider simulation box is required.

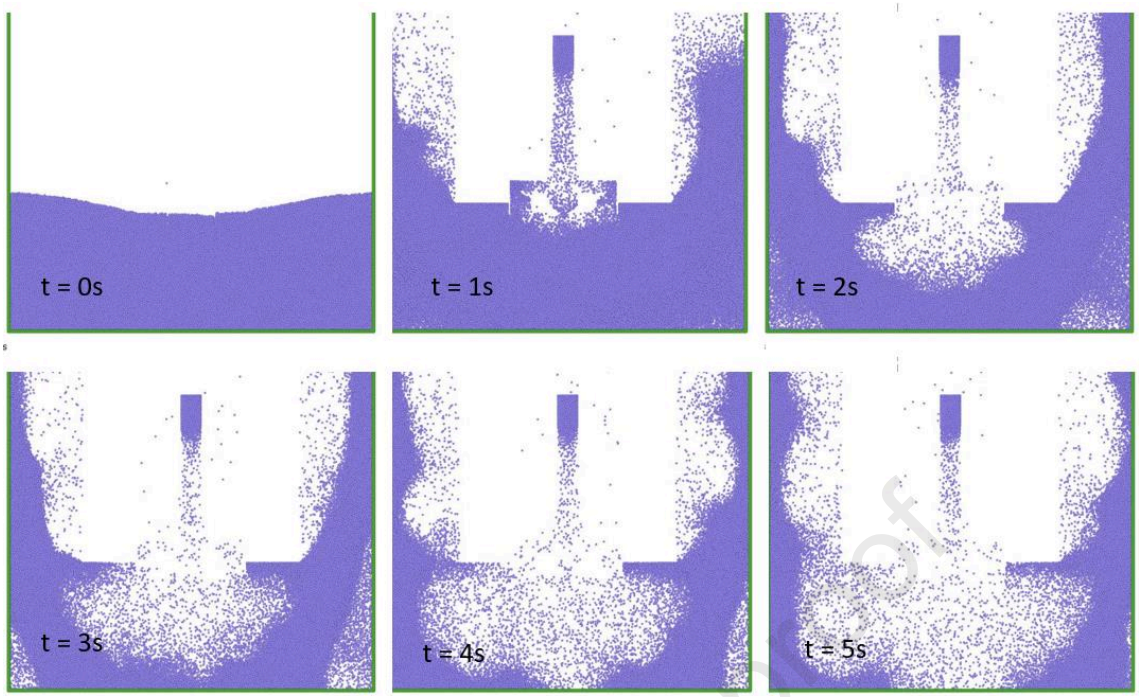

Figure 6-2 Example of sampling on an asteroid at various sampling running times at 100rpm rotation speed. Showing the affected area beneath the sampling region.

If results from sampling through a larger simulation box allow a sufficient sample collection, then the maturity of the concept is advanced. If an insufficient sample is provided, then a modification to the sample distribution might need to be made. For instance, sample acquisition is performed only once with the requirements of providing enough samples for the five ovens; and samples are stored in a primary sample canister before being distributed to the ovens. However, this potential solution might need a larger volume envelope, which might be challenging to be implemented in the current CubeSat volume budget. To counter this issue, the use of one reusable oven might be necessary, rather than the five single-use ovens in the carousel; so thus will provide more volume to be used by the modified sample acquisition system.

To explore the impact of particle-particle interactions, it is crucial to conduct a range of simulations. One approach is to assess the outcomes obtained by incorporating the characteristics of different particles such as Moon, Martin, CM, CI, and sand properties. Furthermore, performing a laboratory experiment with sand on Earth and comparing its behaviour to the simulated results would provide valuable insights into the accuracy of the simulations.

This study has not explored the potential effects of employing a polydisperse distribution on the performance of sampling. It is necessary to compare the performance of a simplified monodisperse distribution with a more representative particle distribution in order to assess any potential influence. One notable concern is the occurrence of a jammed funnel. However, it is possible that incorporating a specific gap between the screws of each Archimedes screw could serve as a filtering mechanism, allowing for the exclusion and acceptance of particles of specific sizes. Consequently, this approach may mitigate the risk of jamming. Nonetheless, additional research is necessary to explore and validate this possibility.

All simulations involve the insertion of an equal number of particles. Varying the particle count can impact the sampling performance. However, the critical factor lies in the depth at which the paddle is immersed within the particles, known as the paddle-particles depth. The quantity of particles may influence the extent to which the paddle is buried within the regolith, subsequently affecting the sampling performance during the initial seconds of operation. Therefore, it is essential to conduct this simulation in order to observe and analyse the sampling performance accurately.

6.2 Summary

This work presents a complete process from planning to finally being able to verify the compatibility of the sample acquisition concept in a microgravity environment via discrete element modelling simulation. Analysis of its accuracy and drawback of the results are also presented. A set of simulations to observe sampler compatibility at various locations was also performed along with potential future work to address the characteristics of the sampling concept.

6.3 Conclusion

The introduction of an Archimedes screw into the counter-rotating sampler concept has demonstrated enhanced sample collection performance. However, further investigations are required to comprehensively understand the implementation and limitations of this sampling mechanism on asteroids and planetary bodies with higher gravitational forces.

Additionally, additional studies are necessary to assess the capability of supplying samples to the five ovens within the overall mission scenario. Preliminary examinations have explored the sampler's performance in the event of failure, such as when one set of paddles becomes jammed, revealing that the sampler can still provide samples albeit at a reduced efficiency level.

Regarding the application of this concept to other planetary bodies, simulations conducted at alternative In-Situ Resource Utilization (ISRU) locations have highlighted limitations inherent to the sampling concept. To address these limitations, a suggestion has been made to redesign the internal structure of the oven to mitigate the challenges encountered in higher gravity environments. However, further research is essential to evaluate the feasibility of implementing the sampling concept on other planetary bodies.

7 Acknowledgement

The authors would like to express appreciation to Lembaga Pengelola Dana Pendidikan (Indonesia Endowment Funds for Education) for their financial support of this PhD research project. The funding provided by this institution was instrumental in enabling us to carry out this study. This research has the potential to contribute to the advancement of knowledge in our field and we hope that our findings will be of benefit to the academic community and society at large.

8 References

Barnouin, O.S. *et al.* (2019) 'Shape of (101955) Bennu indicative of a rubble pile with internal stiffness', *Nature Geoscience*, 12, pp. 247–252. Available at: https://doi.org/https://doi.org/10.1038/s41561-019-0330-x.

Bonitz, R. (2012) 'The brush wheel sampler - A sampling device for small-body touch-and-go missions', in *2012 IEEE Aerospace Conference*. IEEE, pp. 1–6. Available at: https://doi.org/10.1109/AERO.2012.6187049.

Flynn, G.J. *et al.* (2018) 'Physical properties of the stone meteorites: Implications for the properties of their parent bodies', *Geochemistry*, 78(3), pp. 269–298. Available at: https://doi.org/10.1016/j.chemer.2017.04.002.

Gautier, F. *et al.* (2020) 'Drop Your Thesis! 2018 results: 4.74 seconds of microgravity conditions to enable future cubesat landings on asteroids', *Acta Astronautica*, 176, pp. 139–155. Available at: https://doi.org/10.1016/j.actaastro.2020.06.003.

Gundlach, B. and Blum, J. (2013) 'A new method to determine the grain size of planetary regolith', *Icarus*, 223(1), pp. 479–492. Available at: https://doi.org/10.1016/j.icarus.2012.11.039.

Ibrahim, E.-M. (2012) *The elastic properties of carbonaceous chondrites*. University of Calgary.

Jedicke, R. *et al.* (2022) 'Optimized continuous-thrust round-trip trajectories to ultra-low Δv ISRU targets', *Planetary and Space Science*, 211, p. 105407. Available at: https://doi.org/10.1016/j.pss.2021.105407.

Just, G.H. *et al.* (2020) 'Parametric review of existing regolith excavation techniques for Moon In Situ Resource Utilisation (ISRU) and recommendations for future excavation experiments', *Planetary and Space Science*, 180, p. 104746. Available at: https://doi.org/10.1016/j.pss.2019.104746.

Kargel, J.S. (1996) 'Market Value of Asteroidal Precious Metals in an Age of Diminishing Terrestrial Resources', in. Engineering, Construction, and Operation in Space Engineering, Construction, and Operation in Space. Available at: https://doi.org/10.1061/40177(207)111.

LAMMPS (2020) *LAMMPS Region Command*. Available at: https://lammps.sandia.gov/doc/region.html.

Machuca, P., Sánchez, J.P. and Greenland, S. (2019) 'Asteroid flyby opportunities using semi-autonomous CubeSats: Mission design and science opportunities', *Planetary and Space Science*, 165, pp. 179–193. Available at: https://doi.org/10.1016/j.pss.2018.11.002.

Macke, R.J., Consolmagno, G.J. and Britt, D.T. (2011) 'Density, porosity, and magnetic susceptibility of carbonaceous chondrites', *Meteoritics & Planetary Science*, 46(12), pp. 1842–1862. Available at: https://doi.org/10.1111/j.1945-5100.2011.01298.x.

Müller, T.G. *et al.* (2017) 'Hayabusa-2 mission target asteroid 162173 Ryugu (1999 JU 3): Searching for the object's spin-axis orientation', *Astronomy & Astrophysics*, 599, p. A103. Available at: https://doi.org/10.1051/0004-6361/201629134.

Rosenberg, S.D., Guter, G.A. and Miller, F.E. (1964) 'Manufacture of Oxygen from Moon Materials', *Annals of the New York Academy of Sciences*, 123(2), pp. 1106–1122.

Sandeep, C. *et al.* (2019) 'Experimental study on the coefficient of restitution of grain against block interfaces for natural and engineered materials', *Canadian Geothenical Journal* [Preprint].

Schäfer, C.M. *et al.* (2017) 'Numerical simulations of regolith sampling processes', *Planetary and Space Science*, 141, pp. 35–44. Available at: https://doi.org/10.1016/j.pss.2017.04.015.

Scott, G.D. and Kilgour, D.M. (1969) 'The density of random close packing of spheres', *Journal of Physics D: Applied Physics*, 2(6), p. 311. Available at: https://doi.org/10.1088/0022-3727/2/6/311.

Walsh, K.J. *et al.* (2022) 'Assessing the Sampleability of Bennu's Surface for the OSIRIS-REx Asteroid Sample Return Mission', *Space Science Reviews*, 218(4), p. 20. Available at: https://doi.org/10.1007/s11214-022-00887-2.

Wei, Q. *et al.* (2021) 'Simulation analysis and experiment of sampling process of wheel brush sampler based on discrete element method', *Journal of Physics: Conference Series*, 2137(1), p. 012058. Available at: https://doi.org/10.1088/1742-6596/2137/1/012058.

Highlights

- Numerical Simulations on granular behaviour interaction to a sample acquisition system on asteroids (microgravity) and other space bodies.
- Basic counter rotating paddles/bristles with the addition of Archimedes screw as the sample acquisition system.
- Sampling rate between various counter rotating paddles geometry are analysed.
- The addition of Archimedes screw at the paddles increases the sampling rate.
- Small-sized (CubeSat compatible) sample acquisition system

About the authors:

Elioenai Sitepu, PhD – Current a faculty member in Master of Industrial Engineering at Bina Nusantara University, Indonesia. Pursued his PhD in Cranfield University, UK. Prior to joining BINUS, he performed a research project awarded and funded by European Space Agency (ESA) under Drop Your Thesis Program, characterising CubeSat landing on asteroids by utilising the Zarm Drop Tower.

Professor David Cullen - Professor of Astrobiology and Space Biotechnology, Centre for Autonomous and Cyberphysical Systems, Cranfield University. His involvement with the space sector began with a chance encounter with a member of the UK Beagle 2 Mars lander team and a discussion about environmental biosensors being relevant to detecting life on Mars. This discussion led to the proposing, selection and then development of the multiplexed immunoassay-based Life Marker Chip instrument for the ESA ExoMars rover until the instrument de-selection during the major ExoMars mission revision in 2012. He continues a range of activities involving the development of space relevant technology and instrumentation and especially within areas relevant to astrobiology and biosciences. Current applications include the exploitation of CubeSat spacecraft as platforms to perform microgravity and space radiation bioscience experiments and development of early in situ demonstrations of ISRU on Near Earth Asteroids via CubeSat payloads

Declaration of interests

☒ The authors declare that they have no known competing financial interests or personal relationships that could have appeared to influence the work reported in this paper.

☐ The authors declare the following financial interests/personal relationships which may be considered as potential competing interests:

Granular sample collection simulation via counter rotating wheels sampler for small-sized system at reduced gravity environment

Sitepu, Elioenai

2023-09-13

Sitepu E, Cullen D. (2023) Granular sample collection simulation via counter rotating wheels sampler for small-sized system at reduced gravity environment. Planetary and Space Science, Volume 237, November 2023, Article number 105778

https://doi.org/10.1016/j.pss.2023.105778